A Generalised Kelvin-Voigt Damping Model for Geometrically-Nonlinear Beams

Marc Artola *, Andrew Wynn † and Rafael Palacios ‡
Department of Aeronautics, Imperial College London, London, UK, SW7 2AZ

Strain-rate based damping is investigated in the strong form of the intrinsic equations of three-dimensional geometrically exact beams. We use a generalisation of Kelvin-Voigt damping, often limited in the literature to linear or two-dimensional beam models, to the three-dimensional case, including rigid-body motions. The result is an elegant infinite-dimensional description of geometrically exact beams that facilitates theoretical analysis and sets the baseline for any chosen numerical implementation. In particular, we derive the dissipation rates and equilibrium points of the system for the most general case and for one in which a first order approximation of the resulting damping terms is taken. Finally, numerical examples are given which validate the resulting model against a nonlinear damped Euler-Bernoulli beam (where detail is given on how an equivalent description using our intrinsic formulation is obtained) and support the analytical results of energy decay rates and equilibrium solutions caused by damping. Throughout the paper, the relevance of damping higher order terms, arising from the geometrically-exact description, to the accurate prediction of its effect on the dynamics of highly flexible structures is highlighted.

Nomenclature

$C(s)$	=	beam sectional compliance matrix
$C_\tau(s)$	=	damping coefficients matrix
$D_0(s)$, $D_1(s)$, $D_2(s)$	=	matrices of linearised damping terms
$E(s)$	=	initial curvature/twist matrix
$\epsilon(t)$	=	beam total energy
$\eta(s)$	=	damping coefficient
$\boldsymbol{e}_i(s), \quad i = 1, 2, 3$	=	beam local frame of reference basis
$\boldsymbol{e}_i^*, \quad i = 1, 2, 3$	=	global frame of reference basis
$\boldsymbol{f}(s,t)$	=	sectional resultant forces vector

*Graduate research assistant, Room CAGB 308, South Kensington Campus, Student Member AIAA (marc.artola16@imperial.ac.uk)
†Senior Lecturer, Room CAGB 340, South Kensington Campus (a.wynn@imperial.ac.uk)
‡Professor in Computational Aeroelasticity, Room CAGB 338, South Kensington Campus, Associate Fellow AIAA (r.palacios@imperial.ac.uk)

$\boldsymbol{f}_e(s,t)$	=	external local forcing vector
$\boldsymbol{\gamma}(s,t)$	=	local strains vector
$\boldsymbol{\kappa}(s,t)$	=	local curvatures vector
$\boldsymbol{\kappa}_0(s)$	=	initial curvatures vector
L	=	beam's unstressed arclength
$M(s)$	=	beam sectional inertia matrix
$\boldsymbol{m}(s,t)$	=	sectional resultant moments vector
$\mu(s)$	=	beam mass per unit length
s	=	curvilinear coordinate defining beam's elastic axis
t	=	time
$T(s,t)$	=	transformation matrix from local to global frame of references
$u(t)$	=	forcing input
$\boldsymbol{v}(s,t)$	=	local translational velocity vector
$\boldsymbol{\omega}(s,t)$	=	local angular velocity vector
$\boldsymbol{x}_1(s,t)$	=	intrinsic translational/angular velocity state
$\boldsymbol{x}_2(s,t)$	=	intrinsic sectional resultant force/moment state

I. Introduction

Theoretical analysis of damping in structural dynamics is a notable challenge and often two more practical and approximate strategies to damp oscillations and dissipate energy are employed: the first one relies on the assumption of proportional/viscous damping while the second one introduces an ad-hoc numerical damping.

The first approach has been, undoubtedly, the most commonly used ever since Rayleigh introduced the idea of viscous damping [1] and it builds on the physical concept that forces arising to damping oppose velocity. The classical description of structural dynamics $M\ddot{\boldsymbol{x}} + K\boldsymbol{x} = \boldsymbol{0}$ describes the vibration of undamped structures, where the vector $\boldsymbol{x}$ gathers all the structure's degrees of freedom and M and K are the mass and stiffness matrices (with both M and/or K possibly $\boldsymbol{x}$-dependent to account for nonlinear effects). Subsequently, damping is introduced by adding a term $D\dot{\boldsymbol{x}}$ to the previous equation, where it is assumed that $D = \alpha M + \beta K$, with $\alpha, \beta \geq 0$. This is not only a simple way to model damping but it also offers remarkable analysis advantages as, for instance, modal analysis is facilitated [2]. However, damping mechanisms in real structures arise from more complex mechanisms and hence viscous/proportional damping can fail to predict accurately its real effect on the overall dynamics. Significant effort is still put in the quest for identifying both viscous [3] and non-viscous [4] mechanisms experimentally.

With the second approach, damping is added artificially to the equations by employing certain time-marching

integration schemes, as it is usually done with the Newmark-β scheme [5, 6]. However, this methodology does not build on any kind of physical mechanism but is a mere numerical artefact employed to stabilise solvers, hence dismissing any attempt on understanding the role of damping in the dynamics.

As opposed to viscous/proportional damping, where the source of damping is external (e.g. friction with surrounding fluid), structural damping is an internal energy dissipation mechanism (e.g. friction between atomic particles that make up the structure). Hence, modelling of structural damping requires a deeper understanding of the damping mechanisms. It has been found that in linear elastic materials a generic model can be often utilised by means of the following constitutive law [7], which defines the characteristics of a viscoelastic material by relating the temporal derivatives of both stresses (σ) and strains (ϵ)

$$\sum^{N} a_n \frac{\partial^n}{\partial t^n}\sigma = \sum^{M} b_m \frac{\partial^m}{\partial t^m}\epsilon, \tag{1}$$

with constant coefficients $a_n,\ b_m$. Different analytical models stem from this constitutive law, such as the strain-rate based damping (Kelvin-Voigt, where $N = 0$ and $M = 1$ are chosen) or time hysteretic damping models, accounting for past loading time-histories. Spatial hysteretic models can also be obtained by considering spatial derivatives in (1). An early thorough study of the four most common physical damping mechanisms is found in [8], although damping modelling remains still an active field of research, with a recent comprehensive study addressing the identification [9] and analysis of non-viscous [10] damping mechanisms. All these analytical models, based on physical principles, have been used alongside linear beam models [11–13], for the complexity of the resulting system is still amenable to mathematical manipulation and theoretical analysis.

Recent advances in lightweight composite materials and the ongoing quest for improving aerodynamic efficiency of aircraft and wind turbine blades have led to a dramatic increase in slenderness, and hence, flexibility. Design and control of such aerostructures demands the use of geometrically nonlinear models in order to capture nonlinear effects due to the large deflections and rotations arising from the increased flexibility. Many are the reasons why theoretical analysis of damping within the field of three dimensional dynamics of highly flexible structures is disregarded and more practical strategies such as proportional damping or numerical dissipation are considered. A fundamental reason is the complexity of the underlying equations of motion, which are nonlinear. In the particular area of aeroelasticity [14–16], another motivation leading to the underestimation of more realistic structural models is the fact that aerodynamic damping plays a much more significant role in the overall dynamics. However, this reasoning is based on linear assumptions and extending it to the nonlinear scenario remains still of unclear validity.

Due to the aforementioned lack of analysis, understanding of the physical mechanisms of damping within these structures is yet very limited. A very recent paper addressing geometrically nonlinear beams [17] shows how the Kelvin-Voigt model is introduced in a 3D mixed-formulation (based on strains, velocities and displacements), resulting from the combination of a Variational Asymptotic Method, which effectively condenses the sectional dynamics using

the beam's centreline, and a Geometrically-Exact Beam Theory (GEBT) formulation. In this paper, we modify, instead, the strong form of this GEBT, the intrinsic nonlinear beam formulation [18] (expressed in terms of linear and angular velocities and sectional resultant forces/moments), to accommodate Kelvin-Voigt damping. Writing the structural equations in such energy variables appears to be gaining relevance over the last few years [19, 20] since the resulting systems possesses particular structures (e.g. symmetry, first-order time and spatial derivatives, quadratic nonlinearities) which ease mathematical manipulation and energy-based control strategies. Another particularity is that rigid-body motions are inherently embedded in the solution space, thanks to expressing the motions through velocities, avoiding the explicit addition of the rigid-body equations, which proves very valuable for modelling free-flying vehicles. It has also been found that this set of equations admits a rather natural modal-based projection which allows constructing low-order models very suitable for control synthesis [21]. In our case, the resulting system is a compact infinite-dimensional 3D description of damped geometrically-exact beam equations, which facilitates theoretical analysis and makes a much needed contribution in the poorly explored large-deflections area, where models are often limited to axial vibrations [22, 23] or two-dimensional nonlinear models [24]. A summarised theoretical description of this new approach was given in [21], however a more detailed version is included here for completeness. Furthermore, the focus in this paper is on the numerical investigation and the practical implications of the novel damped nonlinear intrinsic equations.

As it is suggested by (1), and further investigated in this paper, modifying the constitutive relationship between forces and strains to account for damping may have a significant effect on the internal force/moments distribution. In particular, nonlinear terms arising from damping (despite (1) being linear) arise due to couplings of cross-product nature between forces and velocities within the formulation. The relevance of these higher order terms to the overall dynamics is studied throughout the paper and they are eventually deemed paramount to an accurate description of highly flexible structures. Specifically, we investigate the energy decay rates and the resulting equilibrium solutions imposed by the addition of structural damping in the full nonlinear scenario and in the case where these higher order terms involving damping are neglected. Numerical simulations are later performed to exemplify and confirm the theoretical findings.

II. Original nonlinear intrinsic beam equations

The dynamics of slender composite beams are described by the intrinsic, geometrically-exact beam theory of Hodges. The equations were initially derived from Hamilton's principle using a mixed formulation: generalised strains and curvatures were used to express the beam's elastic potential energy and generalised linear and angular momenta coordinates to describe the kinetic energy [25]. The closed form of the equations, which needs of constitutive relationships between generalised momenta coordinates and sectional linear and angular velocities and between generalised strains and force/moment sectional resultants, was given in [18]. Under small strain assumptions, these constitutive laws are linear and, by appropriate choice of coefficients (typically done experimentally for small-amplitude tests), they can also account for sectional warping effects. This formulation, following the notation

introduced in [26], uses two vector states, with components in local coordinates, namely the linear and angular inertial velocities vector $\boldsymbol{x}_1(s,t) := [\boldsymbol{v}^\top \, \boldsymbol{\omega}^\top]^\top : [0,L] \times \mathbb{R}_+ \to \mathbb{R}^6$ and the force and moment sectional resultants vector $\boldsymbol{x}_2(s,t) := [\boldsymbol{f}^\top \, \boldsymbol{m}^\top]^\top : [0,L] \times \mathbb{R}_+ \to \mathbb{R}^6$. The curvilinear spatial coordinate is denoted by s, which defines the beam's elastic axis, and t is used to denote time. The arc-length of the undeformed and unloaded structure is L. Using prime $(\bullet)'$ and dot $(\dot{\bullet})$ superscripts to denote partial derivatives with respect to s and t, respectively, the equations read

$$M\dot{\boldsymbol{x}}_1 - \boldsymbol{x}_2' - E\boldsymbol{x}_2 + \mathcal{L}_1(\boldsymbol{x}_1)M\boldsymbol{x}_1 + \mathcal{L}_2(\boldsymbol{x}_2)C\boldsymbol{x}_2 = \boldsymbol{f}_e, \tag{2}$$

$$C\dot{\boldsymbol{x}}_2 - \boldsymbol{x}_1' + E^\top \boldsymbol{x}_1 - \mathcal{L}_1^\top(\boldsymbol{x}_1)C\boldsymbol{x}_2 = 0, \tag{3}$$

together with natural boundary conditions (i.e. no boundary forcing)

$$x_{1i}(0,t)x_{2i}(0,t) = 0, \quad x_{1i}(L,t)x_{2i}(L,t) = 0, \qquad i = 1,\ldots,6, \tag{4}$$

where, for example, x_{1i} denotes the i^{th} entry of the vector x_1 (that is, at a given boundary, either a velocity or force component can be prescribed). Matrices $M(s) : \mathbb{R} \to \mathcal{S}_6^{++}$ and $C(s) : \mathbb{R} \to \mathcal{S}_6^{+}$ are the mass and compliance matrices, with $\mathcal{S}_6^{++}$ and $\mathcal{S}_6^{+}$ denoting the set of positive definite and semi-definite symmetric matrices of $\mathbb{R}^{6\times6}$, respectively. These matrices define the aforementioned linear relationships between the intrinsic variables and the generalised linear and angular momenta $\boldsymbol{p}$, $\boldsymbol{h} \in \mathbb{R}^3$ and generalised strains and curvatures $\boldsymbol{\gamma}$, $\boldsymbol{\kappa} \in \mathbb{R}^3$ as follows:

$$\begin{pmatrix} \boldsymbol{p} \\ \boldsymbol{h} \end{pmatrix} = M \begin{pmatrix} \boldsymbol{v} \\ \boldsymbol{\omega} \end{pmatrix} = M\boldsymbol{x}_1, \qquad \begin{pmatrix} \boldsymbol{\gamma} \\ \boldsymbol{\kappa} \end{pmatrix} = C \begin{pmatrix} \boldsymbol{f} \\ \boldsymbol{m} \end{pmatrix} = C\boldsymbol{x}_2. \tag{5}$$

The matrix $E(s) : \mathbb{R} \to \mathbb{R}^{6\times6}$ gathers information on the initial curvature and pre-twist $\boldsymbol{\kappa}_0 \in \mathbb{R}^3$ (i.e. for beams with curvature in an unloaded configuration, such as arched structures)

$$E = \begin{pmatrix} \widetilde{\boldsymbol{\kappa}}_0 & 0 \\ \widetilde{\boldsymbol{e}}_1 & \widetilde{\boldsymbol{\kappa}}_0 \end{pmatrix}, \tag{6}$$

where $\boldsymbol{e}_1 = [1,0,0]^\top$ is the first vector of a body-attached frame of reference (with origin at the beam's elastic axis and in which all variables and matrices are expressed), tangent to the beam's elastic axis. The tilde superscript $\widetilde{\boldsymbol{a}}$ denotes the vector product matrix operator, defined as $\widetilde{\boldsymbol{a}}\boldsymbol{b} = \boldsymbol{a} \times \boldsymbol{b}$, for $\boldsymbol{a}, \boldsymbol{b} \in \mathbb{R}^3$. The linear operators $\mathcal{L}_1, \mathcal{L}_2 : \mathbb{R}^6 \to \mathbb{R}^{6\times6}$ are defined as

$$\mathcal{L}_1(\boldsymbol{x}_1) = \begin{pmatrix} \widetilde{\boldsymbol{\omega}} & 0 \\ \widetilde{\boldsymbol{v}} & \widetilde{\boldsymbol{\omega}} \end{pmatrix}, \qquad \mathcal{L}_2(\boldsymbol{x}_2) = \begin{pmatrix} 0 & \widetilde{\boldsymbol{f}} \\ \widetilde{\boldsymbol{f}} & \widetilde{\boldsymbol{m}} \end{pmatrix}. \tag{7}$$

External forces and moments per unit length, acting along the structure (e.g. aerodynamic or gravitational forces), are

gathered in the vector $\boldsymbol{f}_e : [0, L]\times\mathbb{R}_+ \to \mathbb{R}^6$. Prescribed motions or forces at a boundary are enforced as $\boldsymbol{x}_{1i}(s_\partial, t) = u(t)$ or $\boldsymbol{x}_{2i}(s_\partial, t) = u(t)$, with $u(t) : \mathbb{R}_+ \to \mathbb{R}$ a function of time and $s_\partial \in \{0, L\}$. The total energy (kinetic and potential) of the system is given by

$$\epsilon(t) = \frac{1}{2}\left\langle \boldsymbol{x}_1, M\boldsymbol{x}_1\right\rangle + \frac{1}{2}\left\langle \boldsymbol{x}_2, C\boldsymbol{x}_2\right\rangle, \tag{8}$$

with time derivative

$$\dot{\epsilon}(t) = \left\langle \boldsymbol{x}_1, \boldsymbol{f}_e\right\rangle + \boldsymbol{x}_1^\top \boldsymbol{x}_2\Big|_0^L, \tag{9}$$

where $\langle \boldsymbol{x}, \boldsymbol{y}\rangle$ denotes the $L^2([0, L])^6$-inner product. We note that, provided boundary conditions (4) are satisfied and there is no external forcing $\boldsymbol{f}_e$, energy is conserved.

III. Structural damping model

In this section we show how the Kelvin-Voigt model for structural damping is added to the original nonlinear intrinsic beam equations (2)–(3). We start by rewriting (2)–(3) prior to the introduction of the linear strain-force relationship (5), which expresses the dynamics of geometrically exact beams using velocities, $\boldsymbol{x}_1$, strains and curvatures $\boldsymbol{\gamma}$, $\boldsymbol{\kappa}$ and sectional force and moment resultants $\boldsymbol{f}$, $\boldsymbol{m}$:

$$M\dot{\boldsymbol{x}}_1 - \left(\begin{smallmatrix}\boldsymbol{f}\\ \boldsymbol{m}\end{smallmatrix}\right)' - E\left(\begin{smallmatrix}\boldsymbol{f}\\ \boldsymbol{m}\end{smallmatrix}\right) + \mathcal{L}_1(\boldsymbol{x}_1)M\boldsymbol{x}_1 + \mathcal{L}_2\left(\left(\begin{smallmatrix}\boldsymbol{f}\\ \boldsymbol{m}\end{smallmatrix}\right)\right)\left(\begin{smallmatrix}\boldsymbol{\gamma}\\ \boldsymbol{\kappa}\end{smallmatrix}\right) = \boldsymbol{f}_e, \tag{10}$$

$$\left(\begin{smallmatrix}\dot{\boldsymbol{\gamma}}\\ \dot{\boldsymbol{\kappa}}\end{smallmatrix}\right) - \boldsymbol{x}_1' + E^\top \boldsymbol{x}_1 - \mathcal{L}_1^\top(\boldsymbol{x}_1)\left(\begin{smallmatrix}\boldsymbol{\gamma}\\ \boldsymbol{\kappa}\end{smallmatrix}\right) = 0. \tag{11}$$

Then, the strain-force constitutive law in (5), which closes the problem, is modified according to the Kelvin-Voigt model of damping, where the stresses (here force/moment resultants, due to the sectional condensation) receive and additional contribution proportional to the strains time-derivative:

$$\begin{pmatrix}\boldsymbol{f}\\ \boldsymbol{m}\end{pmatrix} = C^{-1}\begin{pmatrix}\boldsymbol{\gamma}\\ \boldsymbol{\kappa}\end{pmatrix} + C_\tau C^{-1}\frac{\partial}{\partial t}\begin{pmatrix}\boldsymbol{\gamma}\\ \boldsymbol{\kappa}\end{pmatrix} = \boldsymbol{x}_2 + C_\tau\frac{\partial \boldsymbol{x}_2}{\partial t} \tag{12}$$

for a suitable choice of damping matrix C_τ, whose entries should be determined by a sectional condensation exercise similar to that required to obtain sectional inertia and compliance properties M and C. An insight on how to proceed to obtain such matrices is given in [17]. Note that the definition of $\boldsymbol{x}_2$ is restricted now to refer uniquely to the product $\boldsymbol{x}_2 = C^{-1}\left(\begin{smallmatrix}\boldsymbol{\gamma}\\ \boldsymbol{\kappa}\end{smallmatrix}\right)$, conversely to the original case, where $\boldsymbol{x}_2$ referred both to the force/moment sectional resultants $\left(\begin{smallmatrix}\boldsymbol{f}\\ \boldsymbol{m}\end{smallmatrix}\right)$ and to the product $C^{-1}\left(\begin{smallmatrix}\boldsymbol{\gamma}\\ \boldsymbol{\kappa}\end{smallmatrix}\right)$, since a one-to-one relationship was established between the instantaneous forces/moments and generalised strains. Here, $C_\tau C^{-1} \in \mathbb{S}^6_+$, where C_τ is the damping coefficients matrix. As deduced from (12), C_τ has dimensions of time, which gives time scales that characterise the damping of the viscoelastic material.

A. Damped full nonlinear equations

By replacing the force and moment terms in (10) using the modified constitutive law (12), the damped version of the nonlinear intrinsic beam equations are

$$M\dot{\boldsymbol{x}}_1 - (\boldsymbol{x}_2 + C_\tau\dot{\boldsymbol{x}}_2)' - E(\boldsymbol{x}_2 + C_\tau\dot{\boldsymbol{x}}_2) + \mathcal{L}_1(\boldsymbol{x}_1)M\boldsymbol{x}_1 + \mathcal{L}_2(\boldsymbol{x}_2 + C_\tau\dot{\boldsymbol{x}}_2)C\boldsymbol{x}_2 = \boldsymbol{f}_e, \tag{13}$$

$$C\dot{\boldsymbol{x}}_2 - \boldsymbol{x}_1' + E^\top\boldsymbol{x}_1 - \mathcal{L}_1^\top(\boldsymbol{x}_1)C\boldsymbol{x}_2 = 0. \tag{14}$$

We note that the compatibility equation (14) remains unchanged by the new constitutive law, since no force/moment terms are present. A similar approach is taken in [17], where strains/curvatures terms in the variational form are not modified and are obtained from forces/moments using the time-integrated version of (12).

In the damped case, natural boundary conditions (4) are replaced by

$$\boldsymbol{x}_{1i}(s_\partial, t)\,(\boldsymbol{x}_2(s_\partial, t) + C_\tau\dot{\boldsymbol{x}}_2(s_\partial, t))_i = 0, \qquad i = 1, \ldots, 6,\ s_\partial \in \{0, L\}, \tag{15}$$

since the addition of structural damping modifies the force and moment distributions. Similarly to the undamped case, if velocity is prescribed at any of the boundaries $\boldsymbol{x}_{1i}(s_\partial, t) = u(t)$. However if force is prescribed we have $[\boldsymbol{x}_2(s_\partial, t) + C_\tau\dot{\boldsymbol{x}}_2(s_\partial, t)]_i = u(t)$, where $[\cdot]_i$ denotes the ith entry of the vector.

Energy rate

Under this damping model, we now proceed to evaluate the new energy rate (9) for the case where no external forces nor boundary control are present (i.e. $\boldsymbol{f}_e = \boldsymbol{0}$ and boundary conditions (15) hold). Differentiating (8) and using (13)–(14),

$$\begin{aligned}
\dot{\epsilon} = {} & \langle \boldsymbol{x}_1, M\dot{\boldsymbol{x}}_1\rangle + \langle \boldsymbol{x}_2, C\dot{\boldsymbol{x}}_2\rangle = \\
& \left\langle \boldsymbol{x}_1, (\boldsymbol{x}_2 + C_\tau\dot{\boldsymbol{x}}_2)'\right\rangle + \langle \boldsymbol{x}_1, E\,(\boldsymbol{x}_2 + C_\tau\dot{\boldsymbol{x}}_2)\rangle - \langle \boldsymbol{x}_1, \mathcal{L}_1(\boldsymbol{x}_1)M\boldsymbol{x}_1 + \mathcal{L}_2\,(\boldsymbol{x}_2 + C_\tau\dot{\boldsymbol{x}}_2)\,C\boldsymbol{x}_2\rangle \\
& + \left\langle \boldsymbol{x}_2, \boldsymbol{x}_1'\right\rangle - \left\langle \boldsymbol{x}_2, E^\top\boldsymbol{x}_1\right\rangle + \left\langle \boldsymbol{x}_2, \mathcal{L}_1^\top(\boldsymbol{x}_1)C\boldsymbol{x}_2\right\rangle.
\end{aligned}$$

Leveraging the skew-symmetric properties of E, $\mathcal{L}_1$ and $\mathcal{L}_2$, it can be easily shown that, for any $\boldsymbol{x}_1, \boldsymbol{x}_2 \in \mathbb{R}^6$, the following results hold

$$\langle \boldsymbol{x}_1, E\boldsymbol{x}_2\rangle - \left\langle \boldsymbol{x}_2, E^\top\boldsymbol{x}_1\right\rangle = 0, \tag{16}$$

$$\boldsymbol{x}_1^\top\mathcal{L}_1(\boldsymbol{x}_1) = 0, \tag{17}$$

$$\boldsymbol{x}_2^\top\mathcal{L}_1^\top(\boldsymbol{x}_1) = \boldsymbol{x}_1^\top\mathcal{L}_2(\boldsymbol{x}_2). \tag{18}$$

Consequently,

$$\begin{aligned}\dot{\epsilon} &= \left\langle \boldsymbol{x}_1, (\boldsymbol{x}_2 + C_\tau \dot{\boldsymbol{x}}_2)' \right\rangle + \langle \boldsymbol{x}_1, E C_\tau \dot{\boldsymbol{x}}_2 \rangle - \langle \boldsymbol{x}_1, \mathcal{L}_2 (C_\tau \dot{\boldsymbol{x}}_2) C \boldsymbol{x}_2 \rangle + \left\langle \boldsymbol{x}_2 + C_\tau \dot{\boldsymbol{x}}_2, \boldsymbol{x}_1' \right\rangle - \left\langle C_\tau \dot{\boldsymbol{x}}_2, \boldsymbol{x}_1' \right\rangle \\ &= \boldsymbol{x}_1^\top (\boldsymbol{x}_2 + C_\tau \dot{\boldsymbol{x}}_2)\big|_0^L + \langle \boldsymbol{x}_1, E C_\tau \dot{\boldsymbol{x}}_2 \rangle - \langle \boldsymbol{x}_1, \mathcal{L}_2 (C_\tau \dot{\boldsymbol{x}}_2) C \boldsymbol{x}_2 \rangle - \left\langle C_\tau \dot{\boldsymbol{x}}_2, \boldsymbol{x}_1' \right\rangle .\end{aligned}$$

Using boundary conditions (15), substituting $\boldsymbol{x}_1'$ using (14), and employing again the properties of the E and $\mathcal{L}$ operators (16)–(18) we arrive at

$$\dot{\epsilon} = - \langle C_\tau \dot{\boldsymbol{x}}_2, C \dot{\boldsymbol{x}}_2 \rangle \leq 0, \tag{19}$$

where the final inequality holds since $C_\tau C^{-1} \in \mathbb{S}^6_+$.

Unforced equilibrium solutions

They are obtained using a Lyapunov stability argument. We use the energy of the system ϵ as our Lyapunov candidate function, since we note that $\epsilon > 0$ for all $\boldsymbol{x}_1 \neq \boldsymbol{0}$ and $\boldsymbol{x}_2 \neq \boldsymbol{0}$ and $\dot{\epsilon} \leq 0$. Assuming $C_\tau C^{-1} \succ 0$ and $\boldsymbol{f}_e = \boldsymbol{0}$, we have that $\dot{\epsilon} < 0$ for any $\dot{\boldsymbol{x}}_2 \neq \boldsymbol{0}$, and using LaSalle's Invariance Principle, which states that trajectories converge to the largest invariant set in $\{\boldsymbol{x}_1, \boldsymbol{x}_2 \mid \dot{\epsilon} = 0\}$, solutions to (13)-(15) converge to trajectories given by

$$\dot{\boldsymbol{x}}_2 = \boldsymbol{0} \quad \Rightarrow \quad \boldsymbol{x}_1' = E^\top \boldsymbol{x}_1 - \mathcal{L}_1^\top(\boldsymbol{x}_1) C \boldsymbol{x}_2. \tag{20}$$

Solutions described by (20) are rigid-body type steady trajectories (i.e. $\dot{\boldsymbol{x}}_2 = \boldsymbol{0}$ implies no variation of the elastic deformations) with constant energy ϵ, where the structure is allowed to have some remaining stress distribution due to gyroscopic forces appearing from steady rotations. A numerical example of these particular solutions is given in section V.B. Furthermore, by (20) it is also implied that if one of the boundaries is clamped (i.e. $\boldsymbol{x}_1(s_\partial) = \boldsymbol{0}$), then $\boldsymbol{x}_1(s,t) \to \boldsymbol{0}$ at every s as $t \to \infty$.

We also note that, when the nonlinear terms arising from damping forces are retained, solutions to the damped intrinsic equations remain invariant with rigid body displacements (solutions to the original intrinsic equations are invariant due to the main variables being vector fields) since by (19) no dissipation occurs and by (12) the solution is unaffected when the motions are purely rigid, which are characterised precisely by $\dot{\boldsymbol{x}}_2 = 0$, that is, strains and curvatures remain constant.

B. Nonlinear equations with linearised damping effect

Here, we describe a linearised version of the damped intrinsic beam equations (13)–(14), where original geometrically nonlinear terms are kept intact but those arising from damping are neglected. As it will be shown, this linearised damping produces solutions which are still energy-dissipative, even when coupled with the nonlinear structural model.

We proceed by taking a first order expansion of the strain-rate dependent force $C_\tau \dot{\boldsymbol{x}}_2$ in (12) using the linear terms in (3)

$$C_\tau \dot{\boldsymbol{x}}_2 = C_d C \dot{\boldsymbol{x}}_2 \approx C_d(\boldsymbol{x}_1' - E^\top \boldsymbol{x}_1), \tag{21}$$

where we have introduced the matrix $C_d = C_\tau C^{-1}$. Now, the nonlinear intrinsic beam equations with linearised damping contribution read

$$M\dot{\boldsymbol{x}}_1 - \boldsymbol{x}_2' - E\boldsymbol{x}_2 + \mathcal{L}_1(\boldsymbol{x}_1)M\boldsymbol{x}_1 + \mathcal{L}_2(\boldsymbol{x}_2)C\boldsymbol{x}_2 = D_0\boldsymbol{x}_1 + D_1\boldsymbol{x}_1' + D_2\boldsymbol{x}_1'' + \boldsymbol{f}_e, \tag{22}$$

$$C\dot{\boldsymbol{x}}_2 - \boldsymbol{x}_1' + E^\top \boldsymbol{x}_1 - \mathcal{L}_1^\top(\boldsymbol{x}_1)C\boldsymbol{x}_2 = 0, \tag{23}$$

with natural boundary conditions

$$\boldsymbol{x}_{1i}(s_\partial, t)\left(\boldsymbol{x}_2(s_\partial, t) + C_d(s_\partial)\left(\boldsymbol{x}_1'(s_\partial, t) - E^\top \boldsymbol{x}_1(s_\partial, t)\right)\right)_i = 0, \qquad i = 1, \ldots, 6,\ s_\partial \in \{0, L\}, \tag{24}$$

and where substitution of (21) into (13) has led to the appearance of the linearised damping matrices

$$D_0 = -(C_d E^\top)' - EC_d E^\top, \qquad D_1 = C_d' - C_d E^\top + EC_d, \qquad D_2 = C_d. \tag{25}$$

As revealed by (22), linear Kelvin-Voigt damping is naturally written in terms of the spatial derivatives of the material velocities. This is a consequence of the compatibility equation between strains/curvatures and translational/angular velocities in the intrinsic formulation (23).

For the particular case in which structural properties (i.e. C and C_τ) are constant in space, C_d is block diagonal and therefore written as $C_d = \mathrm{diag}(C_f, C_m)$ and there is no initial curvature ($\boldsymbol{\kappa}_0 = \boldsymbol{0}$), the matrices (25) reduce to

$$D_0 = \begin{pmatrix} 0 & 0 \\ 0 & \widetilde{\boldsymbol{e}}_1 C_f \widetilde{\boldsymbol{e}}_1 \end{pmatrix},\ D_1 = \begin{pmatrix} 0 & C_f \widetilde{\boldsymbol{e}}_1 \\ \widetilde{\boldsymbol{e}}_1 C_f & 0 \end{pmatrix},\ D_2 = \begin{pmatrix} C_f & 0 \\ 0 & C_m \end{pmatrix}, \tag{26}$$

where $D_0 \in \mathcal{S}_6^-$, $D_2 \in \mathcal{S}_6^+$ and D_1 is skew-symmetric.

Finally, if forces are to be prescribed at any of the boundaries, now $\left[\boldsymbol{x}_2(s_\partial, t) + C_d\left(\boldsymbol{x}_1'(s_\partial, t) - E^\top \boldsymbol{x}_1(s_\partial, t)\right)\right]_i = u(t)$ holds.

Energy rate

With this linearised damping model we compute the new energy rate (9), under the same assumptions as in the nonlinear scenario: no external forces nor boundary control are present (that is, $\boldsymbol{f}_e = \boldsymbol{0}$ and (24) hold). We start by

using the result (9), which gives now

$$\dot{\epsilon} = \boldsymbol{x}_1^\top \boldsymbol{x}_2\big|_0^L + \left\langle \boldsymbol{x}_1, D_0\boldsymbol{x}_1 + D_1\boldsymbol{x}_1' + D_2\boldsymbol{x}_1'' \right\rangle . \tag{27}$$

Expanding each of the terms in the expression above

$$\boldsymbol{x}_1^\top \boldsymbol{x}_2\big|_0^L = -\boldsymbol{x}_1^\top C_d \left(\boldsymbol{x}_1' - E^\top \boldsymbol{x}_1\right)\big|_0^L , \tag{28}$$

$$\langle \boldsymbol{x}_1, D_0\boldsymbol{x}_1 \rangle = -\left\langle \boldsymbol{x}_1, EC_dE^\top \boldsymbol{x}_1 \right\rangle + \left\langle \boldsymbol{x}_1', C_dE^\top \boldsymbol{x}_1 \right\rangle + \left\langle \boldsymbol{x}_1, C_dE^\top \boldsymbol{x}_1' \right\rangle - \boldsymbol{x}_1^\top C_dE^\top \boldsymbol{x}_1\big|_0^L , \tag{29}$$

$$\left\langle \boldsymbol{x}_1, D_1\boldsymbol{x}_1' \right\rangle = \left\langle \boldsymbol{x}_1, C_d'\boldsymbol{x}_1' \right\rangle - \left\langle \boldsymbol{x}_1, C_dE^\top \boldsymbol{x}_1' \right\rangle + \left\langle \boldsymbol{x}_1, EC_d\boldsymbol{x}_1' \right\rangle , \tag{30}$$

$$\left\langle \boldsymbol{x}_1, D_2\boldsymbol{x}_1'' \right\rangle = -\left\langle \boldsymbol{x}_1, C_d'\boldsymbol{x}_1' \right\rangle - \left\langle \boldsymbol{x}_1', C_d\boldsymbol{x}_1' \right\rangle + \boldsymbol{x}_1^\top C_d\boldsymbol{x}_1'\big|_0^L . \tag{31}$$

The natural boundary conditions (24) have been taken into account to arrive at (28) and integration by parts has been performed to get (29) and (31). Substituting (28)–(31) into (27) results in

$$\dot{\epsilon} = -\left\langle \begin{pmatrix} \boldsymbol{x}_1 \\ \boldsymbol{x}_1' \end{pmatrix}, \begin{pmatrix} 0 & -EC_d^{\frac{1}{2}} \\ 0 & C_d^{\frac{1}{2}} \end{pmatrix} \begin{pmatrix} 0 & -EC_d^{\frac{1}{2}} \\ 0 & C_d^{\frac{1}{2}} \end{pmatrix}^\top \begin{pmatrix} \boldsymbol{x}_1 \\ \boldsymbol{x}_1' \end{pmatrix} \right\rangle \leq 0. \tag{32}$$

Unforced equilibrium solutions

Using the same Lyapunov argument as before, we see that solutions to (22)-(24) now converge to

$$\boldsymbol{x}_1' = E^\top \boldsymbol{x}_1, \tag{33}$$

since we note that (33) forms the null space of the positive-semidefinite matrices appearing in (32): the positive semi-definiteness is given by the product of two transpose matrices with nonzero rank, while if we expand the matrix products in (32) we obtain $\dot{\epsilon} = \int_0^L \left\| C_d^{1/2}(-E^\top \boldsymbol{x}_1 + \boldsymbol{x}_1') \right\|^2 ds$, for which (33) is a zero. In this case, these are rigid-body type steady trajectories with constant energy ϵ too, however limited to pure translational and/or rotation about the longitudinal axis (where no initial curvature is present, i.e. $\boldsymbol{\kappa}_0 = \mathbf{0}$). That is, solutions are rigid-body motions which do not cause any gyroscopic force as it is shown with a numerical example in section V.B. Similarly to the nonlinear case, if one of the boundaries is clamped the structure is completely brought to rest (zero velocity and unstressed configuration).

IV. Relation to standard beam formulations

Since we will validate our damping model with an Euler-Bernoulli testcase [24], it becomes useful to describe how this particular beam model is contained in and obtained from our general nonlinear intrinsic beam formulation. Given the

two dimensional nature of the case we restrict our attention to variables participating in the motion contained in the 1–3 plane, that is v_1, v_3, ω_2 and f_1, f_3, κ_2 with the corresponding inertial and structural properties μ, i_2, EA, EI_2, GA_3 (i.e. mass per unit length, rotary inertia and axial, bending and shear stiffness, respectively) and equal damping coefficient η for each degree of freedom. The nonlinear equations (13)–(14) restricted to this 2D case become

$$\mu\dot{v}_1 - (f_1 + \eta\dot{f}_1)' + \omega_2\mu v_3 - (f_3 + \eta\dot{f}_3)\tfrac{1}{EI_2}m_2 = f_{e1}, \tag{34a}$$

$$\mu\dot{v}_3 - (f_3 + \eta\dot{f}_3)' - \omega_2\mu v_1 + (f_1 + \eta\dot{f}_1)\tfrac{1}{EI_2}m_2 = f_{e3}, \tag{34b}$$

$$i_2\dot{\omega}_2 - (m_2 + \eta\dot{m}_2)' + (f_3 + \eta\dot{f}_3) + (f_3 + \eta\dot{f}_3)\tfrac{1}{EA}f_1 - (f_1 + \eta\dot{f}_1)\tfrac{1}{GA_3}f_3 = m_{e2}, \tag{34c}$$

$$\tfrac{1}{EA}\dot{f}_1 - v_1' - v_3\tfrac{1}{EI_2}m_2 + \omega_2\tfrac{1}{GA_3}f_3 = 0, \tag{34d}$$

$$\tfrac{1}{GA_3}\dot{f}_3 - v_3' - \omega_2 + v_1\tfrac{1}{EI_2}m_2 - \omega_2\tfrac{1}{EA}f_1 = 0, \tag{34e}$$

$$\tfrac{1}{EI_2}\dot{m}_2 - \omega_2' = 0. \tag{34f}$$

Now, the Euler-Bernoulli hypotheses assume that $i_2 \to 0$ and $GA_3 \to \infty$ for finite f_3 (i.e. shear strain tends to zero) and hence damping terms associated to shear strain also vanish $\eta\dot{f}_3 \to 0$. In practice, and in order to avoid the appearance of algebraic expressions, we select i_2 small enough and GA_3 high enough which asymptotically lead us to an Euler-Bernoulli solution (typically a convergence study would be performed to determine appropriate values). Introducing u and w as the axial and transverse displacements, and considering the following kinematic relationships

$$v_1 = \frac{\partial u}{\partial t}, \quad v_3 = \frac{\partial w}{\partial t}, \tag{35}$$

we recover the well-known linear Euler-Bernoulli model by removing all nonlinear terms in (34). Then,

$$\begin{aligned}
&\text{from (34e)} \qquad \omega_2 = -\frac{\partial}{\partial t}\frac{\partial w}{\partial s},\\
&\text{from (34f)} \qquad m_2 = EI_2\frac{\partial^2 w}{\partial s^2},\\
&\text{from (34d)} \qquad f_1 = EA\frac{\partial u}{\partial s},\\
&\text{from (34c)} \qquad f_3 = \frac{\partial}{\partial s}\left(m_2 + \eta\frac{\partial m_2}{\partial t}\right),
\end{aligned}$$

and finally substituting in (34a) and (34b) we arrive at

$$\mu\frac{\partial^2 u}{\partial t^2} - \frac{\partial}{\partial s}\left(EA\frac{\partial u}{\partial s} + \eta EA\frac{\partial^2 u}{\partial t\partial s}\right) = f_{e1}, \tag{36a}$$

$$\mu\frac{\partial^2 w}{\partial t^2} - \frac{\partial^2}{\partial s^2}\left(EI_2\frac{\partial^2 w}{\partial s^2} + \eta EI_2\frac{\partial^3 w}{\partial t\partial s^2}\right) = f_{e3}. \tag{36b}$$

This set of results obtained with the intrinsic formulation can be compared to [24], where von-Kármán's nonlinear strain–displacement relationship is assumed. The model in [24] results in a hybrid between the full nonlinear (34) and the linear Euler-Bernoulli model (36). It can be obtained by removing all nonlinear terms in (34) except for the most relevant one in (34d) ($v_3 \frac{1}{EI_2} m_2$, linked to the geometrical nonlinear inextension effect), which is replaced by an approximate expression resulting in an axial force

$$f_1 = EA\left(\frac{\partial u}{\partial s} + \frac{1}{2}\left(\frac{\partial w}{\partial s}\right)^2\right). \tag{37}$$

For the sake of completeness we also describe how the Timoshenko beam model would be obtained. The hypotheses differ from the Euler-Bernoulli in that GA_3 is finite and $i_2 \neq 0$, hence (34) would already provide a nonlinear Timoshenko beam model. The linear model would be similarly obtained by neglecting all nonlinear terms in (34) but introducing now the rotation angle ϕ and defining the following kinematic equivalences

$$v_1 = \frac{\partial u}{\partial t}, \quad v_3 = \frac{\partial w}{\partial t}, \quad \omega_2 = \frac{\partial \phi}{\partial t}. \tag{38}$$

Then

$$\begin{aligned} &\text{from (34e)} \qquad f_3 = GA_3\left(\frac{\partial w}{\partial s} + \phi\right), \\ &\text{from (34f)} \qquad m_2 = EI_2\frac{\partial \phi}{\partial s}, \\ &\text{from (34d)} \qquad f_1 = EA\frac{\partial u}{\partial s}, \end{aligned}$$

and substituting in (34a), (34b) and (34c) we get to

$$\mu\frac{\partial^2 u}{\partial t^2} - \frac{\partial}{\partial s}\left(EA\frac{\partial u}{\partial s} + \eta EA\frac{\partial^2 u}{\partial t \partial s}\right) = f_{e1}, \tag{39a}$$

$$\mu\frac{\partial^2 w}{\partial t^2} - \frac{\partial}{\partial s}\left(GA_3\left(\frac{\partial w}{\partial s} + \phi\right) + \eta GA_3\left(\frac{\partial^2 w}{\partial t \partial s} + \frac{\partial \phi}{\partial t}\right)\right) = f_{e3}. \tag{39b}$$

$$i_2\frac{\partial^2 \phi}{\partial t^2} - \frac{\partial}{\partial s}\left(EI_2\frac{\partial \phi}{\partial s} + \eta EI_2\frac{\partial^2 \phi}{\partial t \partial s}\right) + GA_3\left(\frac{\partial w}{\partial s} + \phi\right) + \eta GA_3\left(\frac{\partial^2 w}{\partial t \partial s} + \frac{\partial \phi}{\partial t}\right) = m_{e2}. \tag{39c}$$

V. Numerical examples

A. Validation test case

In order to validate the damping model and study its influence on the dynamics of very flexible structures a test case involving a two-dimensional damped nonlinear Euler-Bernoulli beam, investigated in [24], is chosen. In this test case, the dynamic response of the beam under the excitation of a moving transverse harmonic point-force $P(t) = P_0 \sin(\omega t)$ is studied. The beam is set up as seen in Fig. 1, with one of the ends pinned and the other simply supported, free to move axially, where an axial compression load Q is applied. The prestressed state induced by the axial load triggers nonlinear phenomena which makes the setup a rich test case, in which the relevance of both nonlinear terms arising from elastic deformations and from viscoelastic behaviour is revealed.

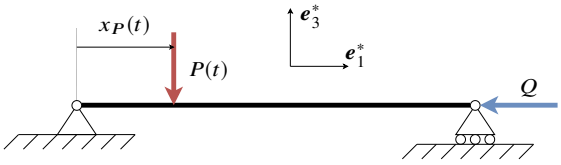

Fig. 1 Setup of the beam subjected to pre-stress caused by an axial compressive force Q and excited with a moving harmonic force $P(t)$

A straight uniform beam with the properties gathered in Table 1 is considered in the reference paper [24]. There, the responses of a linear and nonlinear version of the beam are gathered for diverse excitation frequencies, and attending to their damping model ([24, eq. (8)]), where higher order terms are neglected, it is the case that their results are comparable to our linearised damping model (22)–(24).

Table 1 Beam structural properties of the test case [24]

Length	L	30 m
Mass per unit length	μ	1500 kg/m
Cross sectional area	A	0.36 m^2
Cross sectional moment of inertia	I_2	0.0234 m^4
Young modulus	E	35 GPa
Buckling critical load	Q_{cr}	9,330 kN
First bending mode frequency	ω_b	7.83 rad/s
Damping coefficient*	η	0.01, 0.001, 0.0001 s

In our paper, simulations corresponding to three different models are presented. The nomenclature employed is the following: (*i*) *L. Dyn. – L. Damp.* refers to a linearised version of the nonlinear intrinsic beam equations with (already) linearised damping (22)–(24) about the axial stressed initial configuration $\bar{f}_1 = -Q$, and a linearised displacements evolution equation $\dot{\boldsymbol{r}} = T\boldsymbol{v}$, where T is a transformation matrix from the local to the global frame of references [27].

*Only results corresponding to the intermediate damping coefficient of $\mu = 0.001$ s are provided in [24]. However, higher and lower damping coefficients are considered here to get a deeper insight on the role of nonlinear damping terms.

This set of results is then comparable to those labelled as *linear* in [24]. (*ii*) *NL. Dyn. – L. Damp.* refers to the model (22)–(24) itself, where geometrical nonlinear effects are retained but higher order terms arising from damping are neglected. Its results are comparable to those labelled as *nonlinear* in the reference paper, as long as von-Kármán's assumptions of large transverse displacements, moderate rotations and small strains hold. Finally, (*iii*) *NL. Dyn. – NL. Damp.* refers to the full nonlinear model (13)–(15). For this last model no comparison is available, however, as it will be shown, it is also considered to emphasise the relevant role of the nonlinear damping terms. Full expressions to retrieve rotations and displacements [27] are used for the two *NL. Dyn.* models.

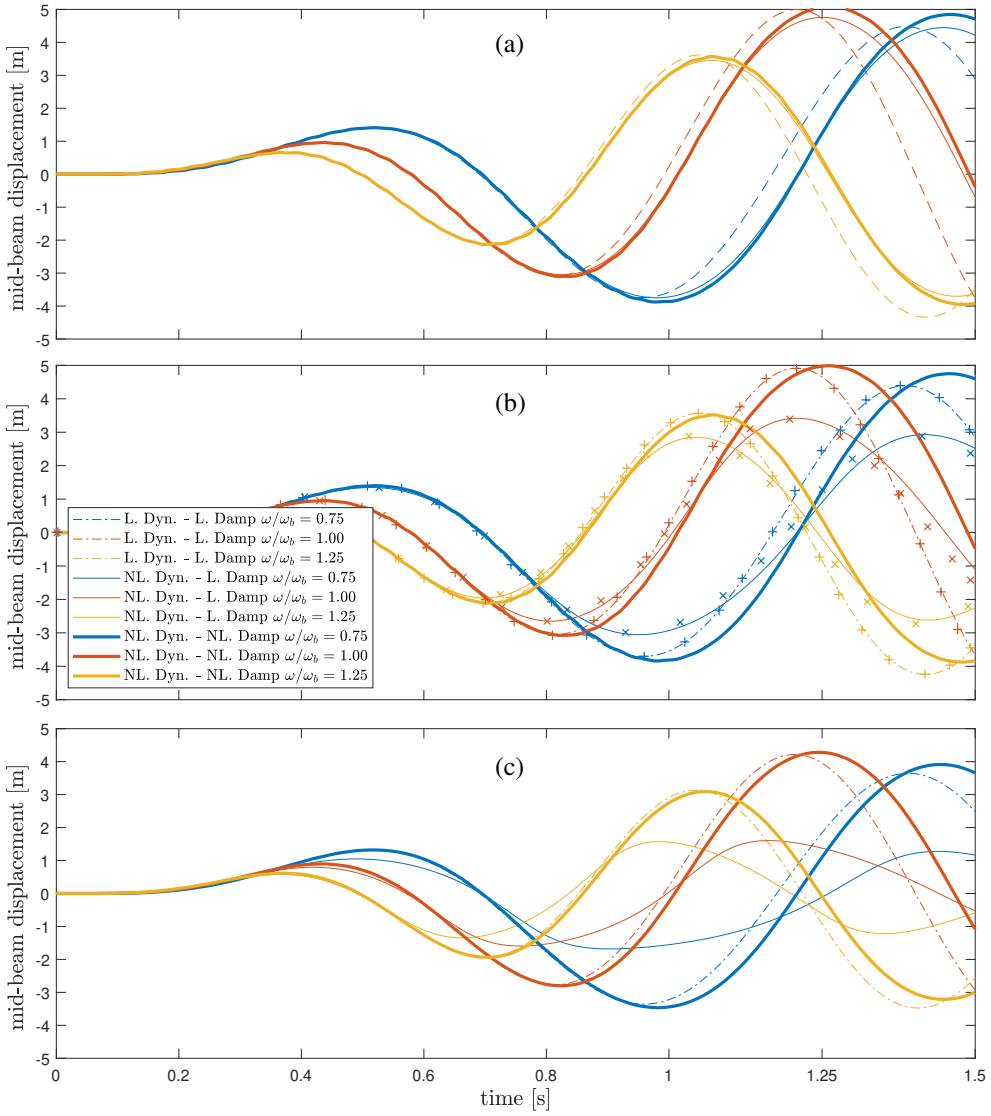

Fig. 2 Mid-beam displacement for damping coefficients of (a) $\eta = 0.0001\,s$, (b) $\eta = 0.001\,s$ and (c) $\eta = 0.01\,s$. Markers (+) and (×) in (b) refer to linear and nonlinear reference results of [24], respectively.

Results shown in Fig. 2 correspond to the particular case [24, Fig. 9c] where an initial pre-stress compression due to an axial force of $Q = 0.1Q_{cr}$, where $Q_{cr} = \frac{\pi^2 EI_2}{L^2}$ is the Euler-Bernoulli buckling critical load, is applied.

Three different excitation frequencies for the harmonic load $P(t)$, corresponding to 0.75, 1.0 and 1.25 times the first bending mode frequency ω_b, are considered and the amplitude of the harmonic force is $P_0 = 2,000\,\mathrm{kN}$. This applied external point-force moves with a constant velocity of $v = 20\,\mathrm{m/s}$, $x_P(t) = 20t$, and the mid-beam deflection, positive downwards, is the studied variable.

In order to simulate an Euler-Bernoulli beam within the intrinsic formulation as indicated by (34) the mass matrix is set to $M = \mathrm{diag}(\mu, \cdot, \mu, \cdot, 10^{-5}\mu I_2/A, \cdot)$ while the compliance matrix $C^{-1} = \mathrm{diag}(EA, \cdot, 10^5 EA, \cdot, EI_2, \cdot)$, where the dots $(\cdot)$ denote that the entries are irrelevant due to the uncoupled (2D) nature of the problem. The 10^5 factors in M and C are used to replicate Euler-Bernoulli hypotheses of negligible rotary inertia and infinite shear rigidity. To match the structural damping, the matrix $C_\tau = \mathrm{diag}(\eta, 0, 0, 0, \eta, 0)$, where equal damping coefficients are chosen for the axial and bending degrees of freedom. Results shown correspond to a finite element discretisation of the structural intrinsic equations, similar to that presented in [28], using quadratic shape functions, with 40 elements, and an implicit mid-point rule integration scheme with a time step $\Delta t = 0.00015\,\mathrm{s}$, for which results are deemed converged.

Gathered in Fig. 2, are the mid-beam vertical displacements for three different damping coefficients. Only results for the intermediate damping value $\eta = 0.001\,\mathrm{s}$ are given in [24], and the comparison is shown in Fig. 2b. We observe an excellent agreement between the reference linear results (+ markers) and those obtained with our *L.Dyn. – L. Damp.* model, across the range of tested excitation frequencies. Regarding the nonlinear case, very satisfactory agreement is also achieved between our *NL.Dyn. – L. Damp.* model results and the reference (× markers), albeit a slight discrepancy can be noticed towards the end of the simulation. This suggests that von-Kármán's strain–displacement relationships do not deviate significantly from those given by the geometrically-exact theory for moderate displacements and the comparison remains appropriate. Results simulating the nonlinear terms arising from damping (neglected in the reference paper) are also included, *NL.Dyn. – NL. Damp.*. The notable discrepancy between them and those where the effect of damping is linearised but geometrically nonlinear effects are still retained, *NL.Dyn. – L. Damp.*, suggests that the role of damping nonlinear terms is, indeed, considerably relevant to the overall dynamics. This could be initially grasped from the difference between equilibrium solutions (20) and (33), which suggests that linearised damping is more dissipative.

Two other scenarios have been simulated, where lower $\eta = 0.0001\,\mathrm{s}$ (Fig. 2a) and higher $\eta = 0.01\,\mathrm{s}$ (Fig. 2c) damping coefficient have been tested. The suggestion that linearised damping produces more dissipative results, already observed in Fig. 2b, is confirmed in Fig. 2c, where a higher damping coefficient leads to an increase in the difference between the responses of the *NL.Dyn. – NL. Damp.* and the *NL.Dyn. – L. Damp.* set of results. However, when the damping coefficient is decreased (Fig. 2a) we observe how both nonlinear responses start to coalesce, distinguishing themselves from the linear response, characterised by its faster dynamics.

B. Response of a damped highly flexible hinged beam

To investigate more in depth the three-dimensional dynamics of beams with the proposed damping model, we simulate the response of a very flexible beam with a ball-joint hinge on one end (3D rotations are allowed) and free on the other end, as seen in Fig. 3, where gravity effects are not simulated to isolate the impact of damping in the dynamics. We use models *NL. Dyn. – L. Damp.* and *NL. Dyn. – NL. Damp.* of the previous section (i.e. both geometrically nonlinear models with linearised and full damping terms, respectively), for which thin line and thick line are used throughout all the figures shown next, following the same thickness code as the one used in the previous section.

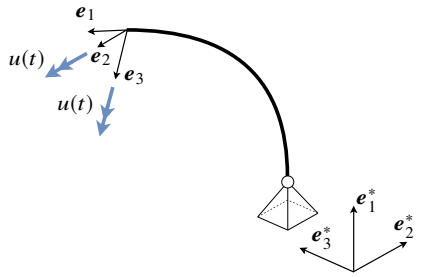

Fig. 3 Setup of the three-dimensional highly-elastic hinged beam subject to two following point torque inputs $u(t)$ applied at the free end.

The structure is a straight uniform beam with mass and compliance matrices $M = \text{diag}(1,\ 1,\ 1,\ 4{\cdot}10^{-4},\ 2{\cdot}10^{-4},\ 2{\cdot}10^{-4})$ and $C = \text{diag}(10^5,\ 5{\cdot}10^3,\ 5{\cdot}10^3,\ 1,\ 1,\ 2)$, all with appropriate units. This choice of structural parameters and boundary conditions provides us with a very flexible structural test case displaying large elastic and rigid-body displacements and rotations. The beam is excited with an input signal $u(t) = \frac{1}{2}\sin(\omega t)\,(\mathcal{H}_0(t) - \mathcal{H}_{0.5}(t))$, where $\mathcal{H}_{t_0}(t)$ is the Heaviside step function at $t = t_0$, with $\omega = 4\pi = 0.82\omega_b$, where ω_b is the frequency of the structure's first bending mode (that is forcing is only active during the first period of the sinusoidal signal, $t \in [0, 0.5]$ s). This input is applied at the free end and with equal magnitude in the $\boldsymbol{e}_2$ and $\boldsymbol{e}_3$ components:

$$m_2(L,t) + \eta E I_2 \omega_2'(L,t) = m_3(L,t) + \eta E I_3 \omega_3'(L,t) = u(t), \tag{40}$$

$$m_2(L,t) + \eta \dot{m}_2(L,t) = m_3(L,t) + \eta \dot{m}_3(L,t) = u(t), \tag{41}$$

for models *NL. Dyn. – L. Damp.* and *NL. Dyn. – NL. Damp.* respectively.

The asymmetry in bending stiffness and the excitation in both transverse directions serve to trigger geometrically nonlinear effects in which torsion and transverse bending motions are coupled. Uniform damping across all degrees of freedom is chosen $C_\tau = \text{diag}(\eta,\ \eta,\ \eta,\ \eta,\ \eta,\ \eta)$, and three different values of $\eta = 0.01,\ 0.001,\ 0.0001$ s are studied. The presented results have been similarly obtained by a FE discretisation of the intrinsic equations, using 40 elements and a time step of $\Delta t = 0.001$ s for a total simulation time of 50 s, for which numerical convergence of the results is achieved.

We first look at the total energy of the beam and the corresponding decay rates for the three studied values of

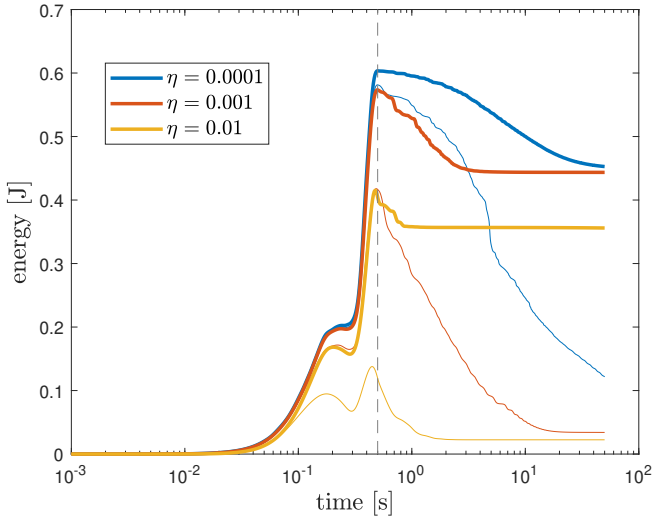

Fig. 4 Total energy (kinetic + potential) of the beam as a function of time for the three different damping coefficients considered. Thick line corresponds to full nonlinear damping, thin line to linearised damping.

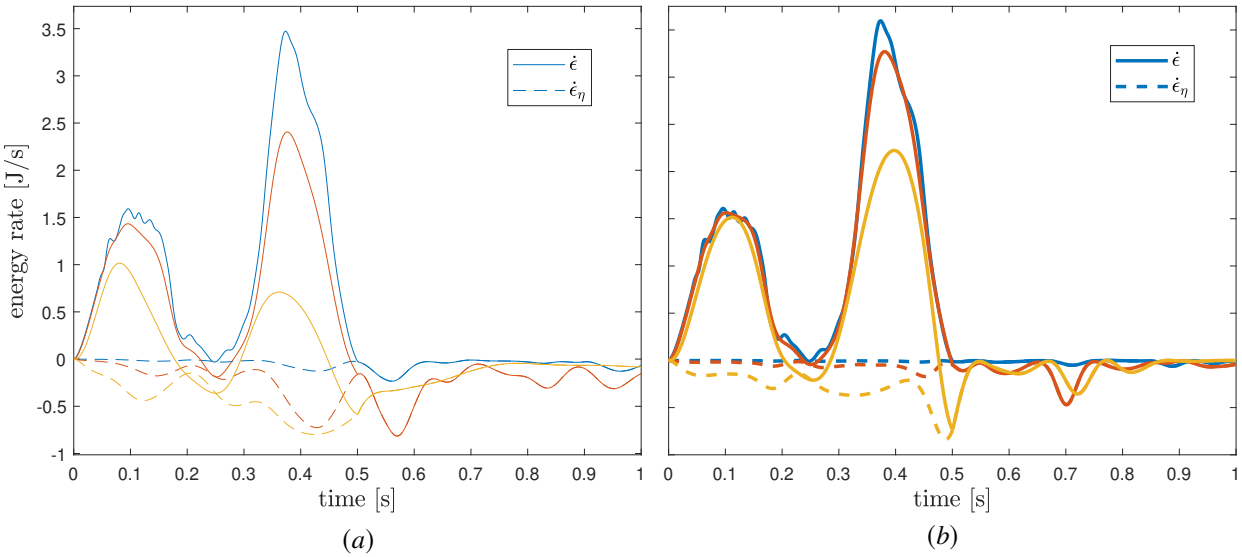

Fig. 5 Energy rate for the first second of simulation for the three different damping coefficients (where color code follows Fig.4) for the (*a*) linearised and the (*b*) full nonlinear damping cases.

damping. Fig. 4 shows the evolution of the beam's total energy for the entire simulation window of 50 s, where logarithmic scale for the abscissa coordinate is used to ease visualisation of the first 0.5 s (with $t = 0.5$ s marked with a vertical dashed line), where the external forcing is active. A first observation is that for every damping coefficient, the model with linearised damping (thin lines) is consistently more dissipative than the full damping terms counterpart, and leads to lower energy states at the end of the simulation. It is also seen that in the case with lower damping coefficient equilibrium conditions are not reached with any of the two models within the simulated window, contrary to the rest of responses, where the energy curve is clearly seen to flaten and eventually reach a constant level.

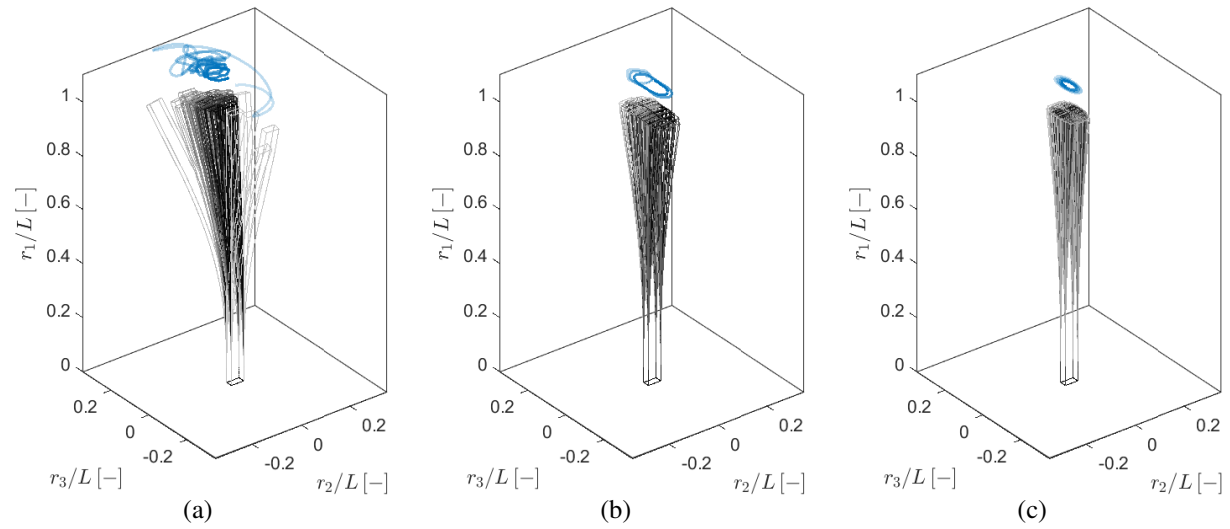

Fig. 6 Snapshots of the beam every 0.1 s for the linearised damping case and $\eta = 0.001$ s, including the projection on a horizontal plane of the tip's displacement trace. Shade darkens with time and (a) $t \in [0, 5]$ s, (b) $t \in [5, 10]$ s, (c) $t \in [10, 15]$ s

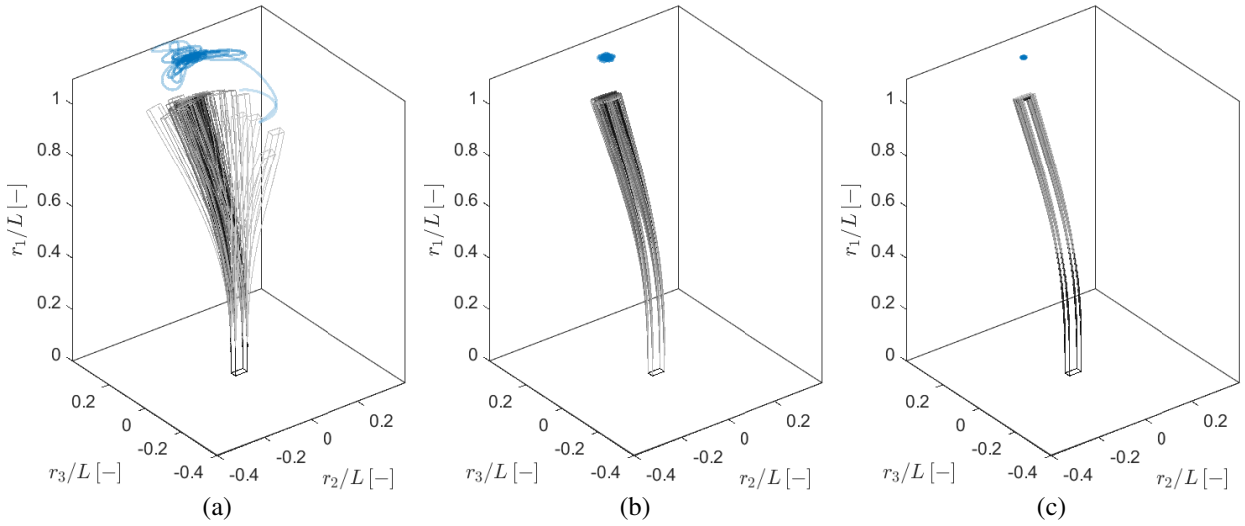

Fig. 7 Snapshots of the beam every 0.1 s for the full nonlinear damping case and $\eta = 0.001$ s, including the projection on a horizontal plane of the tip's displacement trace. Shade darkens with time and (a) $t \in [0, 5]$ s, (b) $t \in [5, 10]$ s, (c) $t \in [10, 15]$ s

The higher dissipation achieved by the linearised damping model is better visualised in Fig. 5a, where the energy decay rates $\dot{\epsilon}(t) = \langle \boldsymbol{x}_1, M\dot{\boldsymbol{x}}_1 \rangle + \langle \boldsymbol{x}_2, C\dot{\boldsymbol{x}}_2 \rangle$ against time are shown for the *NL. Dyn. – L. Damp.* model. When compared to the full-damping counterpart (Fig. 5b), all the curves are lower. That is, when the decay rate is positive during the excitation phase, a lower influx of energy is transmitted to the system, and when it is negative higher dissipation is experienced. Both Fig. 5a and Fig. 5b show the total energy rate of the system in solid line, computed by evaluating the previous general energy rate expression numerically. The dissipation produced by damping $\dot{\epsilon}_\eta$ is also shown in dashed lines and is computed by numerically evaluating the expressions (19), (32). The total energy rate includes the excitation

power influx, and we notice that from $t \geq 0.5$ both dashed and solid lines merge (agreement down to machine precision error), since the external forcing vanishes, which validates the analytically derived energy rates (19)–(32).

Finally, we analyse the equilibrium solutions imposed by damping. We focus attention on the intermediate damping case $\eta = 0.001$ s, for which we observe in Fig. 4 that equilibrium is virtually reached for both models. The solution corresponding to the *NL. Dyn. – L. Damp.* model at the end of the simulation consists of an almost pure rotation around the longitudinal axis with negligible remaining stress. Indeed, the only non-negligible angular velocity component at $t = 50$ s is $\omega_1 = 12.963$ rad/s, which gives a kinetic energy of $\epsilon_K = \frac{1}{2} i_1 L \omega_1^2 = 0.0336$ J matching almost exactly the leftover energy shown in Fig. 4 of $\epsilon = 0.0341$ J. This is in line of (33), which states that the equilibrium set consists of rigid-body type of motions which do not generate gyroscopic effects (i.e. pure translations or rotation about longitudinal axis for straight beams). Since the beam is pinned at one end, longitudinal rotation which is the by-product of the bending-torsion coupling given by the structure's properties is the only admissible equilibrium solution. Snapshots of the beam's displacements, relative to the body-attached frame of reference at the base (to ease visualisation), are given in Fig. 6, where the beam converges to the initial unstressed straight configuration (whilst rotating around $\boldsymbol{e}_1$).

The equilibrium solution for the *NL. Dyn. – NL. Damp.* is more complex, as already suggested by (20). As seen in Fig. 7, the displacements relative to the beam's base rotating frame of reference show a bent configuration about the less stiff axis. This stressed configuration is in equilibrium with the gyroscopic forces induced by a rigid-body rotation of the beam about the hinged joint.

It is therefore apparent that nonlinear terms arising from damping in geometrically nonlinear beams are not negligible, especially where rigid-body motions are present. Not considering them leads to an overestimation of damping, where physical equilibrium solutions, such as those given by (20) and shown in Fig. 7, are inevitably ignored.

VI. Conclusion

An infinite-dimensional formulation for the dynamics of geometrically nonlinear beams with a generalized form of Kelvin-Voigt structural damping has been presented. This development is facilitated by the use of the intrinsic formulation, which describes the beam three-dimensional dynamics using velocities and strains as primary variables. The result is a compact set of partial differential equations that provides a general framework to incorporate measured damping characteristics into the dynamics of beam structures with arbitrary cross sections (including anisotropic materials) with geometrically-nonlinear effects. We note that analytical models to include damping mechanisms are scarce in the literature and very often limited to much simpler configurations and small amplitude dynamics. The proposed formulation builds on the intrinsic theory of beams, and therefore the equations of motions are written in a material frame of reference. This naturally maintains the structure linear constitutive relations into the geometrically-nonlinear dynamics, and in particular, allows the current formulation to identify the coefficients in the damping model from small-amplitude experimental tests.

A theoretical analysis of the decay rates and the equilibrium solutions, consequence of damping, has been performed for the resulting description and for one where a first order approximation to the damping terms has been taken. It is observed that linearisation of the damping terms leads to increased dissipation which eventually removes rotary rigid-body motions from the set of equilibrium solutions. Hence, despite of the increased complexity of the fully–damped model with respect to the linearised one, its use is considered essential for accurate and physically sensible modelling of highly flexible structures, and especially so for those subject to rigid-body motions involving rotations (e.g. wind turbine or helicopter rotor blades). The resulting models have been validated through numerical investigation and several simulations are finally given which support and exemplify the theoretical findings.

Finally, we stress that both the nonlinear intrinsic equations and the Kelvin-Voigt damping model have independently been validated in the literature against experimental evidence for the description of geometrically-exact beam dynamics and structural damping, respectively. As geometrically-nonlinear beam theory still uses linear constitutive relations, we expect that the combination of both models would result in an equally well-founded formulation. Nevertheless, nonlinear experimental validation of the proposed model would be highly valuable to support the theoretical contributions of this paper, and hence it is regarded as a subsequent natural step in the investigation.

Funding Sources

Marc Artola is member of the Innovative Training Network ConFlex. This project has received funding from the European Union's Horizon 2020 research and innovation programme under the Marie Sklodowska-Curie grant agreement No 765579.

References

[1] Rayleigh, L., *Theory of Sound*, 2nd ed., Dover Publications, 1945 (re-issue).

[2] Caughey, T. K., and O'Kelly, M. E. J., "Classical Normal Modes in Damped Linear Dynamic Systems," *Journal of Applied Mechanics*, Vol. 32, No. 3, 1965, pp. 583–588.

[3] Lisitano, D., Bonisoli, E., and Mottershead, J. E., "Experimental Direct Spatial Damping Identification by the Stabilised Layers Method," *Journal of Sound and Vibration*, Vol. 437, 2018, pp. 325 – 339.

[4] Adhikari, S., and Woodhouse, J., "Quantification of Non-Viscous Damping in Discrete Linear Systems," *Journal of Sound and Vibration*, Vol. 260, No. 3, 2003, pp. 499 – 518.

[5] Géradin, M., and Rixen, D., *Mechanical Vibrations: Theory and Application to Structural Dynamics*, 2nd ed., Wiley, 1997.

[6] Hesse, H., Palacios, R., and Murua, J., "Consistent Structural Linearization in Flexible Aircraft Dynamics with Large Rigid-Body Motion," *AIAA Journal*, Vol. 52, No. 3, 2014, pp. 528–538.

[7] Lazan, B., *Damping of Materials and Members in Structural Mechanics*, Pergamon Press, 1968.

[8] Banks, H., and Inman, D., "On Damping Mechanisms in Beams," *NASA Contractor Report*, Vol. 181904, 1989.

[9] Adhikari, S., *Structural Dynamic Analysis with Generalized Damping Models: Identification*, John Wiley and Sons, Ltd, 2014.

[10] Adhikari, S., *Structural Dynamic Analysis with Generalized Damping Models: Analysis*, John Wiley and Sons, Ltd, 2014.

[11] Banks, H., and Wang, Y., "Damping Modeling in Timoshenko Beams," *1992 American Control Conference*, Chicago, IL, USA, 1992, pp. 2139–2143.

[12] Capsoni, A., Viganò, G. M., and Bani-Hani, K., "On Damping Effects in Timoshenko Beams," *International Journal of Mechanical Sciences*, Vol. 73, 2013, pp. 27 – 39.

[13] Wagner, N., and Adhikari, S., "Symmetric State-Space Method for a Class of Nonviscously Damped Systems," *AIAA Journal*, Vol. 41, No. 5, 2003, pp. 951–956.

[14] Wei, X., and Mottershead, J. E., "Aeroelastic Systems with Softening Nonlinearity," *AIAA Journal*, Vol. 52, No. 9, 2014, pp. 1915–1927.

[15] Jiffri, S., Fichera, S., Mottershead, J. E., and Da Ronch, A., "Experimental Nonlinear Control for Flutter Suppression in a Nonlinear Aeroelastic System," *Journal of Guidance, Control, and Dynamics*, Vol. 40, No. 8, 2017, pp. 1925–1938.

[16] del Carre, A., Muñoz-Simón, A., Goizueta, N., and Palacios, R., "SHARPy: A dynamic aeroelastic simulation toolbox for very flexible aircraft and wind turbines," *Journal of Open Source Software*, Vol. 4, No. 44, 2019, p. 1885.

[17] Gupta, M., Sarkar, K., and Hodges, D. H., "Dynamic Analysis of Nonlinear Composite Beams with 3-D Structural Damping," *AIAA Scitech 2019 Forum*, San Diego, CA, USA, 2019, pp. 2139–2143.

[18] Hodges, D. H., "Geometrically Exact, Intrinsic Theory for Dynamics of Curved and Twisted Anisotropic Beams," *AIAA Journal*, Vol. 41, No. 6, 2003, pp. 1131–1137.

[19] Jacob, B., and Zwart, H., *Linear Port-Hamiltonian Systems on Infinite-dimensional Spaces*, Springer, 2012.

[20] Macchelli, A., Melchiorri, C., and Stramigioli, S., "Port-Based Modeling of a Flexible Link," *IEEE Transactions on Robotics*, Vol. 23, No. 4, 2007, pp. 650–660.

[21] Artola, M., Wynn, A., and Palacios, R., "Modal-Based Nonlinear Model Predictive Control for 3D Very Flexible Structures," Under review at *IEEE Transactions on Automatic Control*.

[22] Chen, L. H., Zhang, W., and Liu, Y. Q., "Modeling of Nonlinear Oscillations for Viscoelastic Moving Belt Using Generalized Hamilton's Principle," *ASME. J. Vib. Acoust.*, Vol. 129, No. 1, 2006, pp. 128–132.

[23] Shahruz, S. M., "Stability of a Nonlinear Axially Moving String With the Kelvin–Voigt Damping," *ASME. J. Vib. Acoust.*, Vol. 131, No. 1, 2009, pp. 014501–1–4.

[24] Simsek, M., and Kocatürk, T., "Nonlinear Dynamic Analysis of an Eccentrically Prestressed Damped Beam Under a Concentrated Moving Harmonic Load," *Journal of Sound and Vibration*, Vol. 320, No. 2009, 2009, pp. 235–253.

[25] Hodges, D. H., "A Mixed Variational Formulation Based on Exact Intrinsic Equations for Dynamics of Moving Beams," *International Journal of Solids and Structures*, Vol. 26, No. 11, 1990, pp. 1253 – 1273.

[26] Palacios, R., "Nonlinear Normal Modes in an Intrinsic Theory of Anisotropic Beams," *Journal of Sound and Vibration*, Vol. 330, No. 8, 2011, pp. 1772–1792.

[27] Artola, M., Wynn, A., and Palacios, R., "A Nonlinear Modal-Based Framework for Low Computational Cost Optimal Control of 3D Very Flexible Structures," *2019 18th European Control Conference (ECC)*, Naples, Italy, 2019, pp. 3836–3841.

[28] Palacios, R., Murua, J., and Cook, R., "Structural and Aerodynamic Models in Nonlinear Flight Dynamics of Very Flexible Aircraft," *AIAA Journal*, Vol. 48, No. 11, 2010, pp. 2648–2659.